Nondestructive assessment of the inhibition of enamel demineralization by CO_2 laser treatment using polarization sensitive optical coherence tomography

Dennis J. Hsu
Cynthia L. Darling
Margarita M. Lachica
Daniel Fried
University of California
San Francisco School of Dentistry
Department of Preventative and Restorative Dental Sciences
San Francisco, California, 94143-0758
E-mail: daniel.fried@ucsf.edu

Abstract. Studies have shown that lasers can be used to modify the chemical composition of tooth enamel to render it less soluble. The purpose of this study was to determine if polarization-sensitive optical coherence tomography (PS-OCT) can be used to nondestructively assess the inhibition of demineralization after CO_2 laser irradiation. Human and bovine enamel specimens were irradiated by a microsecond pulsed CO_2 laser operating at a wavelength of 9.3 μm. Some specimen areas were also treated with topical fluoride to create six treatment groups on each sample, including protected surface (no demineralization), protected +laser, laser, fluoride, laser+fluoride, and unprotected surface. Samples were placed in an artificial demineralization solution to create lesions approximately 100–200 μm in depth and were subsequently scanned with a PS-OCT system to assess lesion severity before sectioning for analysis by polarized light microscopy and transverse microradiography for comparison. PS-OCT was able to measure a significant reduction in the integrated reflectivity due to inhibition by the laser on both human and bovine enamel even though the laser modification of the enamel surface did cause an increase in reflectivity and decrease in optical penetration. This study shows that the PS-OCT is well suited for the clinical assessment of caries inhibition after laser treatments. [DOI: 10.1117/1.2976113]

Keywords: CO_2 laser; dental enamel; optical coherence tomography; polarization; demineralization.

Paper 08056R received Feb. 15, 2008; revised manuscript received May 16, 2008; accepted for publication May 20, 2008; published online Sep. 16, 2008. This paper is a revision of a paper presented at the SPIE conference on Lasers in Dentistry XIV, January 2008, San Jose, California. The paper presented there appears (unrefereed) in SPIE Proceedings Vol. 6843.

1 Introduction

Several studies over the past 30 years have indicated that lasers can be used to thermally modify the chemical composition of dental enamel to render it more resistant to acid dissolution and potentially more resistant to dental caries.[1–7] Carbon dioxide laser wavelengths of 9.3 and 9.6 μm have the strongest absorption in dental hard tissues, and a pulse duration in the microsecond range is well matched to the thermal relaxation time of the absorbed laser energy near the tooth surface for those wavelengths. Moreover, other studies have indicated that topical fluoride treatments can work synergistically with the laser treatment to further enhance its inhibitory effect.[8–11] Current techniques for evaluating the efficacy of chemical and thermal (laser) based anticaries methods include transverse microradiography, transverse microhardness, or polarized light microscopy. These methods require destruction of the tooth and hence require test subjects with teeth scheduled for extraction. Therefore, such studies are limited in duration to a maximum of a few months. Natural caries lesions, particularly in occlusal surfaces, require a more extended time for development. One promising new method for the assessment of early caries lesions *in vivo* is polarization-sensitive optical coherence tomography (PS-OCT), which has been successfully used to acquire images of both artificial and natural caries lesions, assess their severity in depth, assess the remineralization of such lesions,[3–5] and determine the efficacy of chemical agents in inhibiting demineralization.[12]

Optical coherence tomography (OCT) is a noninvasive technique for creating cross-sectional images of internal biological structure.[13–15] PS-OCT is a form of OCT that is sensitive to changes in the polarization of the reflected light.[16] We have demonstrated that polarization-sensitive depth-resolved reflectivity measurements can provide a measure of the severity of natural and artificial caries lesions on smooth surfaces and in the occlusal pits and fissures.[17–21] The specular reflectance at the air-enamel interface of the tooth surface is very strong due to the high refractive index of enamel, $n=1.63$,

Address all correspondence to Daniel Fried, PRDS, Univ. of California/San Francisco, 707 Parnassus Ave.—San Francisco, CA 94143; Tel: 415 502 6641; Fax: 415 4760858; daniel.fried@ucsf.edu

1083-3668/2008/13(5)/054027/9/$25.00 © 2008 SPIE

and this poses a particular challenge for OCT. Because the surface reflectivity can be much more intense than the subsurface scattering, it can interfere and overlap the reflectivity from the lesion area to prevent accurate assessment of the lesion depth and severity. If the incident light is linearly polarized, specular surface reflections do not depolarize the incident light and do not interfere with the signal in the orthogonal ($\perp$) polarization state, which can be measured using a PS OCT system. Demineralized areas on the tooth depolarize the incident linearly polarized light, and the reflectivity in the ($\perp$) polarization state can be directly integrated to provide a measure of the lesion severity. By exploiting polarization sensitivity, the reflectivity from all lesion areas can be directly integrated—including the very important surface zones—thus overcoming the interference of strong surface reflections at tooth surfaces, a serious limitation of conventional OCT systems. This is of particular importance for imaging the laser-modified enamel surfaces and the shallow lesions involved in this study. Another concern is that thermal changes in the enamel can induce changes in the birefringence and light-scattering properties of the enamel that can interfere with the ability of PS-OCT to assess the lesion severity. In turn, PS-OCT can potentially be used to determine the depth or thickness of the thermally modified enamel layer to quantify the extent of any peripheral thermal and mechanical damage.

Quantitative light fluorescence (QLF) or laser-induced fluorescence (LIF) has been used to quantify the severity of incipient caries lesions on smooth surfaces *in vivo*.[22–29] The method measures the attenuation of the enamel autofluorescence from beneath the lesion as the lesion increases in severity.[30] The pores in the lesion formed due to demineralization scatter and attenuate the fluorescence that originates from the underlying sound enamel and dentin. The fluorescence loss (in percent) has been compared to the mineral loss integrated with depth, ΔZ (volume percent mineral loss times microns) to give a measure of the lesion severity. However, this method has only been validated for use on smooth surfaces and has not been validated to work on laser treated surfaces.

In a recent study, we demonstrated that PS-OCT can be used to assess the inhibitory effect of fluoride agents and sealants peripheral to orthodontic brackets.[12] The purpose of this paper is to demonstrate that PS-OCT can be used as a nondestructive means of measuring the efficacy of fluoride and CO_2 laser treatments and for measuring the inhibition of lesion formation.

2 Materials and Methods

2.1 *Sample Preparation*

Twelve blocks of dental enamel, approximately $5 \times 3 \times 2$ mm^3, were prepared from twelve extracted bovine tooth incisors, and ten similar-sized human enamel blocks were prepared from extracted human third molar teeth. The enamel surfaces were serial polished to 1 μm using embedded diamond polishing disks. Each enamel sample was partitioned into three regions with the center of each region being treated with the laser using the conditions specified in the next section (see Fig. 1). The middle partition of each sample was covered with a thin layer of acid-resistant varnish in the form of red nail polish (Revlon, New York, New York), which served to protect the sound enamel control area during exposure to the demineralization solution. The middle partitions served as the negative control groups: protected (P) and protected+laser (P+L). A 1.23% acidulated phosphate fluoride foam, Oral B Minute Foam (Gillette, South Boston, Massachusetts) was applied to only one side following treatment with the laser. After allowing exposure for 1 min, the samples were rinsed with deionized water, taking care not to contaminate the nonfluoride, untreated side of the sample. The fluoride treated section served as the fluoride+lesion (F) and fluoride+laser+lesion (F+L) groups. The third section served as the lesion (D) and lesion+laser (D+L) groups. The placement of all six study groups within each sample, lesion (D), lesion plus laser (D+L), sound (P), sound plus laser (P+L), fluoride (F), and fluoride plus laser (F+L), decreases intersample variability. The samples were then cemented to delrin blocks and the sample sides varnished to isolate the enamel surface. After treatment, each of the 22 enamel samples were placed in a demineralization solution for seven days, consisting of a 40 mL aliquot of an acetate buffer solution containing 2.0 mmol/L calcium, 2.0 mmol/L phosphate, and 0.075 mol/L acetate at pH 4.9 maintained at a temperature of 37°C.

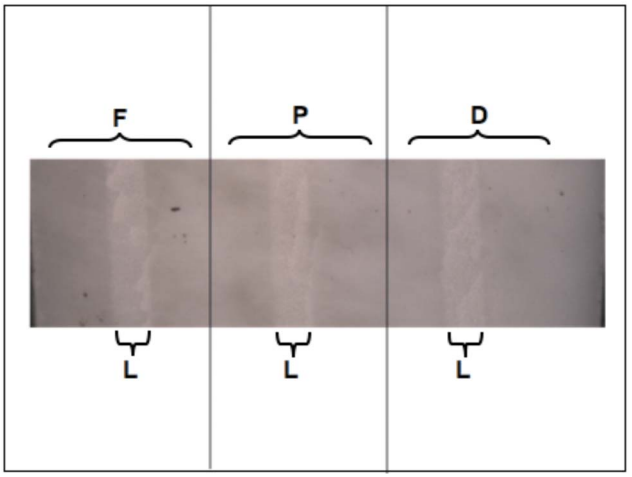

Fig. 1 Reflected light image of a bovine sample following laser irradiation and before coating with varnish and immersion in the demineralization solution showing the three partitioned areas on each sample F, P, and D. The laser-treated areas are in the center of each of the three zones and are labeled (L) in the image and are clearly visible on the surface. The left side is marked F and demarcates the area where the topical fluoride was to be applied; the central zone marked (P) was covered with acid-resistant varnish to protect the surface before immersion in the demineralized solution; and the right side, marked (D), denotes the area that remained unprotected and untreated with fluoride.

2.2 *Laser Treatment*

The enamel samples were irradiated with a transverse excited atmospheric (TEA) pressure CO_2 laser, Impact 2500 (GSI Lumonics, Rugby, United Kingdom) operating at 9.3 μm, a fluence of 1 J/cm^2, an energy of 8 mJ per pulse, and pulse duration of 15 μs. Laser energy calibration and measurement was done using a laser energy/power meter, EPM 1000, Coherent-Molectron (Santa Clara, CA) with an ED-200 Joulemeter from Gentec (Quebec, Canada). A planoconvex ZnSe

lens with a focal length of 100 mm was used to focus the laser to a beam diameter of ~1 mm. The laser beam diameter ($1/e^2$) at the sample position was determined by scanning with a razor blade across the beam. Two- and three-dimensional images of the laser spatial profile was acquired using a Spirocon Pyrocam™ I pyroelectric array (Logan, UT). The laser spatial beam profile showed that the laser was operating in a single spatial mode, Gaussian spatial beam. Irradiation was performed by scanning the laser operating at a repetition rate of 200 Hz continuously at a scanning rate of 3.0 mm/s across the surface of the bovine blocks to create the three irradiation zones (Fig. 1). A computer-controlled stage high-speed motion control system with Newport (Irvine, California) UTM150 and 850G stages and an ESP300 controller was used to create controlled movement of the samples during laser irradiation. For this study, the samples were irradiated without introducing water to the enamel surfaces.

2.3 *PS-OCT System*

An all fiber–based optical coherence domain reflectometry (OCDR) system with polarization-maintaining optical fiber, high-speed piezoelectric fiber stretchers and two balanced InGaAs receivers that was designed and fabricated by Optiphase, Inc., Van Nuys, California, was integrated with a broadband high-power superluminescent diode DL-CS31159A, (Denselight, Singapore) and a high-speed *XY*-scanning system (ESO 300 controller and 850-HS stages, National Instruments, Austin, Texas) and used for *in vitro* optical tomography. The system was configured to provide axial and lateral resolution of approximately 20–25 μm with a signal-to-noise ratio of greater than 40–50 dB. The all-fiber OCDR system is described in more detail in Ref. 31 The PS-OCT system was completely controlled using LabVIEW™ software (National Instruments, Austin, Texas).

2.4 *Polarized Light Microscopy (PLM) and Digital Transverse Microradiography (TMR)*

After the samples were imaged with PS-OCT, the bovine samples were cut into sections approximately 200-μm thick using an Isomet 5000 saw (Buehler, Lake Bluff, Illinois) for PLM and digital TMR. During this step, some thin sections were lost due to the inherent brittleness of enamel coupled with the existence of the induced artificial lesions, which made the samples even more susceptible to fracturing. PLM was carried out using a Scientific Series 7 optical microscope (Westover Scientific, Mill Creek, Washington) with an integrated digital camera, Canon EOS Digital Rebel XT (Canon Inc., Tokyo, Japan). The sample sections were imbibed in water and examined in the brightfield mode with cross polarizers and a red I plate with 500-nm retardation. The lesions appear dark due to the demineralization causing strong scattering that results in a loss of birefringence [Figs. 5(a) and 5(b)]. A custom-built digital TMR system was used to measure mineral loss in the different partitions of the sample. A high-speed motion control system with Newport UTM150 and 850G stages, and an ESP300 controller coupled to a video microscopy and laser targeting system was used for precise positioning of the tooth samples in the field of view of the imaging system.

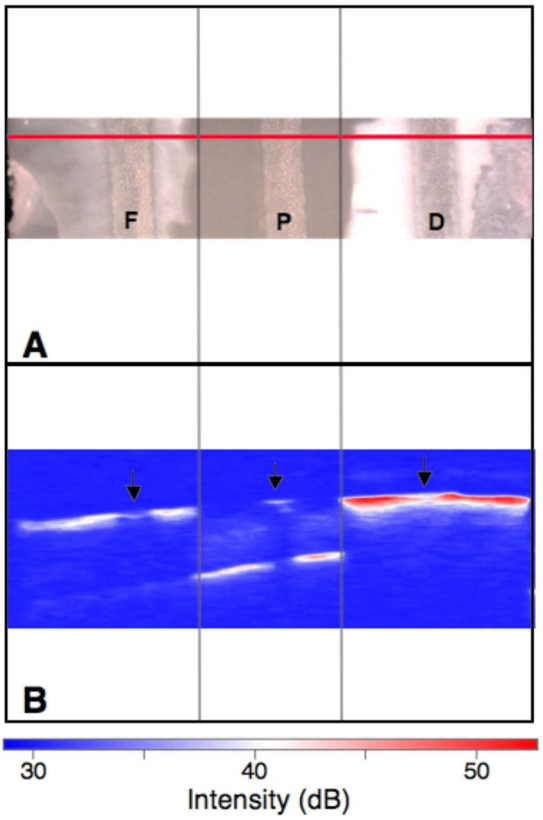

Fig. 2 (a) Reflected light image of a bovine sample following laser treatment with immersion in the demineralization solution with F, P, and D marking the fluoride treated, varnish protected, and unprotected zones, respectively. The gray lines mark the approximate position of those zones on the enamel surface. Areas of more severe mineral loss with increased reflectivity appear white. The red line in (a) indicates the approximate location of the PS-OCT scan (⊥-axis) that is shown in (b). A red-white-blue false color scale in decibel is shown below the scan. More severe lesion areas with the most intense reflectivity/scattering appear in red. In this particular sample, low reflectivity in the sound enamel region (P) does not attenuate the light allowing deeper penetration and the highly reflective DEJ can be seen. The laser zone in the middle of the sound region (P+L) is more reflective and decreases the penetration of the light. The arrows indicate the location of the laser-treated areas. Note the increased lesion severity on the nonfluoride-treated side. (Color online only.)

2.5 *Integrated Reflectivity, Quantitative Mineral Loss Profiles, and Lesion Depth Measurements*

The integrated reflectivity and integrated mineral loss were calculated in each of the six areas for each sample. Line profiles were taken from the orthogonal polarization (⊥-axis) PS-OCT images or b-scans in each of the six regions, and the reflectivity was integrated from the enamel surface to a real depth of 200 μm, yielding the integrated reflectivity, ΔR, of the regions in units of decibels per micron. Previous studies have shown that ΔR correlates directly with the integrated mineral loss (volume % mineral × microns) called ΔZ.[6] Similarly, line profiles were taken from the digital TMR of the thin sections cut along the same position scanned by OCT. X-ray attenuation was converted to volume percent mineral using a sound enamel calibration curve. The line profiles in the four treatment (lesion) areas were subtracted from the sound mineral profiles to yield the integrated mineral loss. The line pro-

files were integrated from the edge of the sample to a depth of 200 μm to give units of ΔZ (volume % $\times$ microns). In some cases, where samples had cavitated, the edge of the sample was linearly extrapolated by calculating the slope along the sample surface and the integration started from the calculated point. This yields a mineral value of $\sim$20–25% in areas where the mineral was completely lost, which is consistent with the mineral volume at which point the enamel matrix collapses. The integrations were performed using Igor Pro software (Wavemetrics, Lake Oswego, Oregon). Prior to taking the line profiles for the OCT images, a 10×10 convolution filter was applied to smooth out the images using the convolution filtering function from the Image Processing package of Igor Pro.

2.6 *Fluorescence Loss Measurements (LIF)*

Enamel surfaces were irradiated with a frequency-doubled diode pumped solid-state Nd:YVO_4 laser (λ=473 nm) DPSS Laser model BLM-50 (Extreme lasers, Houston Texas) with an incident intensity of up to 50 mW. A 500-nm long-pass filter no. C47-616 (Edmund Scientific, Barrington, New Jersey) and a DFK 31AF03 FireWire camera (resolution 1024 $\times$768) from the Imaging Source (Charlotte, North Carolina) were used to image the fluorescence from the surface at wavelengths of >500 nm. Imaging was carried out in the dark to avoid the interference of ambient light. The image contrast was calculated by subtracting the intensity of the fluorescence intensity taken from the treatment areas from the fluorescence intensity of the sound protected region on each sample and subsequently dividing by the fluorescence intensity of the sound-protected region. The fluorescence image contrast varies from 0 to 1 with 1 being very high contrast and 0 being no contrast. A negative contrast indicates that the fluorescence intensity of the treatment area was higher than the fluorescence intensity of the sound-protected region.

3 Results

The surface of a bovine enamel block is shown in Fig. 1 after irradiation by the CO_2 laser. Optical changes caused by melting and recrystallization due to the laser beam are visible to the naked eye and can also be seen on the PS-OCT images before exposure to the demineralization solution. A close up view of a laser-irradiated area is shown in Fig. 3(a) showing the surface morphology and the width of the laser-irradiated zone. The laser beam produces a Gaussian-shaped intensity profile on the enamel surface inducing melting in the center region of the beam and visible changes in the enamel surface in the region of melting. PS-OCT scans taken after the laser treatment and subsequent exposure of the samples to the demineralization solution show that there is also increased resistance to acid dissolution at the outer wings of the laser energy distribution at irradiation intensity levels that are below the threshold that causes visible changes in the enamel surface (i.e., which increase the reflectivity of the enamel in the PS-OCT images). This is clearly apparent from the ($\perp$-axis) PS-OCT image of Fig. 3(b) that shows the laser-treated area on human enamel after exposure to the demineralization solution. The minimum reflectivity is at the wings of the Gaussian distribution of the laser energy. The melted area at the center of the Gaussian beam has an increased reflectivity. The increased

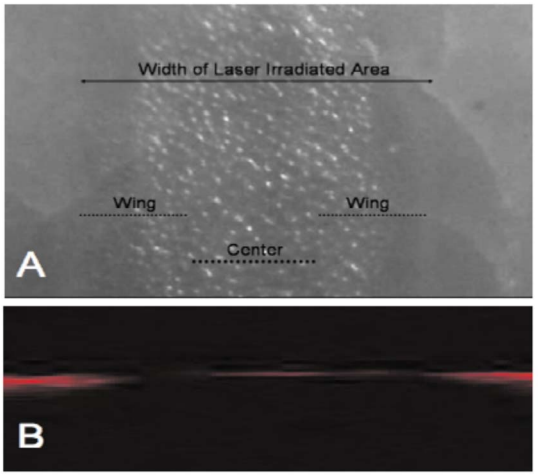

Fig. 3 (a) Reflected light image of a laser-treated area on human enamel before exposure to the demineralization solution at higher magnification zone showing the melted areas and the changed surface morphology. Subsequent ($\perp$-axis) PS-OCT scans, such as the one shown in (b) taken after exposure to the demineralized solution, show that the lowest reflectivity occurs at the "wings" of the Gaussian shaped laser profile at an intensity just below that which melted the enamel surface. The reflectivity is actually higher at the center of the laser-treated area because the enamel transformed by the laser caused an increase in reflectivity near the surface. The area outside the laser zone shows increased reflectivity in depth due to the formation of a lesion (i.e., a zone of demineralized enamel).

reflectivity from the melted area has the potential to interfere with the assessment of the lesion severity. However, the depth of modification is fairly shallow and the rise in reflectivity in the lesion area is substantially higher; therefore, it is still feasible to use PS-OCT to assess lesion severity as is demonstrated in this study.

Reflected light images of bovine and human enamel samples along with the corresponding ($\perp$-axis) PS-OCT images are shown in Figs. 2 and 4. The areas that have the most severe decay or white spot lesions appear more opaque or whiter. The area on the left side, where fluoride was added, is more translucent than the right side, without the fluoride, for the sample shown in Fig. 2. In fact, the lesion was so severe on the right side that part of the enamel surface eroded or cavitated due to extensive demineralization. The areas treated by the laser appear more translucent because demineralization was less severe in those areas compared to the surrounding enamel. A ($\perp$-axis) PS-OCT image or b-scan is shown below for the same sample. A red-white-blue false color scheme is used and the intensity scale in decibel units is shown below the image. The strong areas of scattering/reflectivity, such as lesion areas, and the underlying dentin at the dentin-enamel junction (DEJ) appear red. Areas of high reflectivity not only appear with stronger intensity but also attenuate the penetration of the light deeper into the enamel as well. The DEJ is clearly visible in the protected area near the center, and it is clear that the thermal modification of the enamel at the very center attenuates the light to the degree that the DEJ is not visible at the position directly under the zone melted by the laser. The effect of both the laser and fluoride in inhibiting lesion development are quite dramatic on this sample. The lesion is clearly less severe on the fluoride-treated side, and

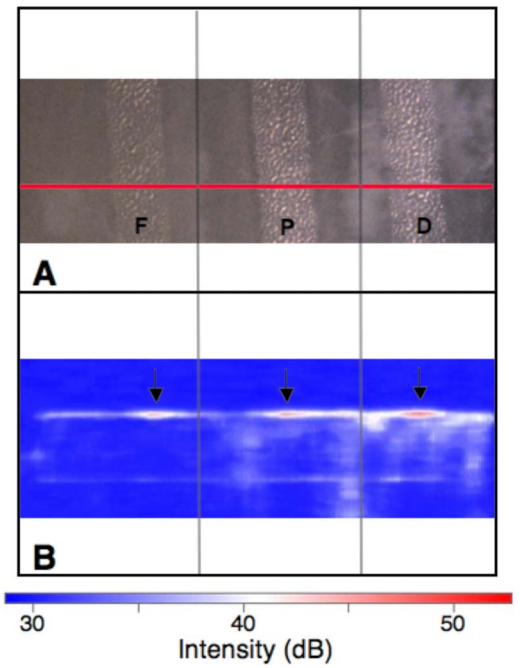

Fig. 4 (a) Reflected light image of a human enamel sample following laser treatment with immersion in the demineralization solution. The red line indicates the approximate location of the PS-OCT scan (⊥-axis) that is shown in (b). Lesions are less severe in the laser-treated areas, and there is no visible cavitation in the lesion areas. (Color online only.)

the lesion is also much less severe in the laser-treated areas on both lesion areas. Lesions are less severe overall on the human enamel samples as can be seen on the example shown in Fig. 4. The lesions are much less severe in the laser-treated areas on this sample as well. The severity of the lesions varied markedly from sample to sample even on the bovine enamel samples that were expected to exhibit a greater uniformity of demineralization. The lesions were typically less severe for the human enamel samples, and the lesions are much less severe in the laser-treated areas and for the fluoride-treated side versus the nonfluoride-treated side.

Figure 5 shows a composite of PLM images taken at 40x magnification across the entire 200-μm-thick section cut from one of the bovine enamel samples along with the corresponding (⊥-axis) PS-OCT scan. In the PLM images, the lesion areas appear dark due to loss of birefringence and the depth of the lesion can be accurately measured. It was difficult to section the samples for PLM and TMR without damage to the fragile lesions, and many samples exhibited loss of mineral from the lesion areas. The sample of Fig. 5 manifested cavitation on the lesion only side (D) due to severe demineralization and lesion damage during the sectioning process on the fluoride side (F). Cavitation is visible on both sides of the laser treated area on the right side (nonfluoride-treated D) in the PS-OCT image before sectioning for histology. A severe but noncavitated lesion is present on the left side (fluoride-treated F) just to the right of the laser-treated area in the black circle. That area is only cavitated in the PLM image, indicating it was damaged during the sectioning process.

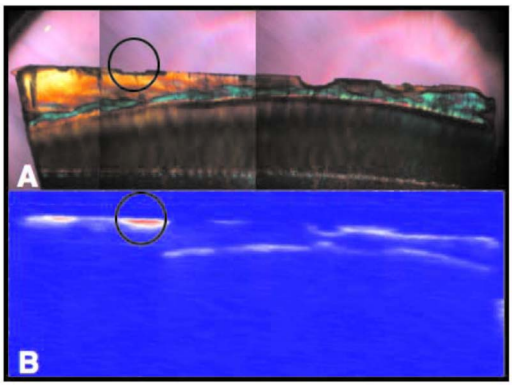

Fig. 5 Polarized light microscopy image (a) and (⊥-axis) PS-OCT scan (b) for a bovine enamel sample that manifested cavitation on the untreated side (no fluoride) due to severe demineralization and lesion damage on the fluoride side due the sectioning process. Cavitation is visible on both sides of the laser-treated area on the right side (no fluoride) in the PS-OCT image before sectioning for histology. A severe but noncavitated lesion is present on the left side (fluoride treated), just to the right of the laser-treated area in the black circle. That area is only cavitated in the PLM image, indicating it was damaged during the sectioning process.

Figure 6 contains a PLM image of a human enamel section along with a TMR image of a bovine enamel section. The laser-treated areas are visible in PLM images even in the sound regions but are not visible in the TMR images. The laser treatments melt and change the structure of the enamel near the surface, causing a loss of birefringence, but had no effect on the overall mineral density. A deep ~180-μm lesion

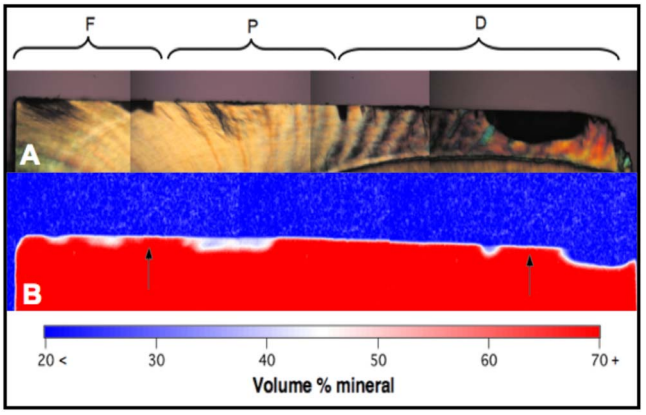

Fig. 6 (a) A composite of several PLM images taken across a human enamel sample with the F, P, and D regions marked. The areas where mineral loss occurred appear darker. The arrows show the position of the laser-treated areas. The laser-treated area at the center of the sound-protected area shows a thick black zone, indicating that the thermal modification of the enamel causes a loss of enamel birefringence to a depth of ~20 μm. The lesion to the right of the laser treated area in (D) is very severe, and the lesion in the fluoride area (F) is clearly visible on both sides of the laser-treated zone. (b) A composite of transverse microradiographs of a different bovine enamel sample with severe demineralization and some cavitation in the unprotected areas is shown. The left and right black arrows mark the position of the laser-treated areas. The right unprotected side (D) of the sample has a large area of cavitation just to the right of the laser-treated zone. A red-white-blue false color scale was also used for TMR to show volume-percent mineral. (Color online only.)

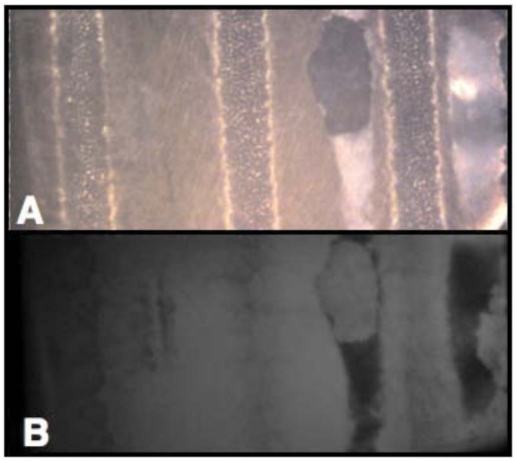

Fig. 7 Reflected light (a) and fluorescence (b) images of a bovine enamel sample following laser treatment and immersion in the demineralization solution. Lesions appear lighter in the reflected light image and darker in the fluorescence image.

is visible on the right side of the unprotected area (D) in the PLM image [Fig. 6(a)] while smaller lesions are visible on the fluoride-treated side. The lack of lesion development in the laser-treated zones is clearly evident (black arrows). The TMR image on another sample shows very similar behavior with the laser-treated areas (black arrows) inhibiting lesion development and more severe demineralization on the right side of the sample. On this particular bovine enamel sample, the lesion was very severe on the right side, resulting in cavitation/erosion.

A reflected light image and a fluorescence image of the surface of a bovine enamel sample are shown in Fig. 7 after laser treatment and immersion in the demineralization solution. The fluorescent images resemble an inverted reflected light image. The highly scattering lesion areas block the fluorescence from the underlying sound enamel and dentin, and those areas manifest reduced levels of intensity (appear dark). In contrast to the reflected light image in which the more severe lesion areas strongly scatter light and cause an increase in intensity. The laser treatment areas on the sound enamel were not significantly darker than the untreated areas, and the florescence intensity in some laser-treated areas was even higher than the sound nonirradiated area, producing a negative fluorescence image contrast for the bovine enamel samples. It is surprising that some of the laser-irradiated areas actually have increased levels of fluorescence compared to the sound enamel. This result was unexpected because the laser-irradiated zones also manifest increased attenuation of the incident near-IR light in the PS-OCT images. It is possible that the melted surface produced by the laser treatment reduced the effective surface roughness of the enamel surface, allowing more fluorescence to exit normal to the enamel surface and thus appear brighter.

The mean integrated reflectivity measured with PS-OCT (depth 200 μm), the mean integrated mineral loss measured with TMR (depth 200 μm), the mean lesion depth measured with PLM, and the mean florescence image contrast between sound and lesion areas are all tabulated in Tables 1 and 2 for human and bovine enamel. Groups with the same letter in each row indicate no significant difference between groups. Sample groups were compared using repeated measures analysis of variance (ANOVA) with a Tukey-Kramer *post hoc* multiple comparisons test. Instat™ from GraphPad software (San Diego, California) was used for the statistical calculations. The mean integrated reflectivity measured with PS-OCT for all the bovine and human enamel groups is plotted in Fig. 8 after subtraction of the integrated reflectivity from the sound area from each of the nonlaser-treated areas and subtraction of the integrated reflectivity from the sound laser-treated area from each of the laser-treated lesion areas. This subtraction was carried out to both correct for the reflectivity of the sound enamel and the increase in reflectivity caused by the laser modification of the enamel surface. The integrated reflectivity was significantly lower for all the groups versus the unprotected lesion (D) area, with the exception of the fluoride only group. We were able to resolve a significant reduction ($p<0.05$) in the integrated reflectivity between regions treated with the combination of laser and fluoride (F+L) versus regions that were completely untreated (D), as

Table 1 Mean (s.d.) values for PS-OCT, TMR, PLM, and LIF for the bovine enamel treatment groups. Sample sizes are indicated in the first column. Groups with same letter in each row are not significantly different ($p>0.05$).

	F	F+L	P	P+L	D	D+L
PS-OCT (dB·μm) (n=9)	1444(692) a,b	752(534) c,d	272(216) c	607(389) c,d	1778(657) b	942(566) a,d
TMR (vol%·μm) (n=7)	1618(777) a	284(368) a	—	—	4114(1911) b	979(789) a
PLM (μm) (n=8)	100(30) a	78(24) a	—	32(10) b	151(29) c	94(42) a
LIF contrast (n=9)	0.54(0.14) a	0.095(0.39) b	—	−0.10(0.16) b	0.62(0.11) a	0.055(0.15) b

Table 2 Mean (s.d.) values for PS-OCT, TMR, PLM, and LIF for the human enamel treatment groups. Sample sizes are indicated in the first column. Groups with same letter in each row are not significantly different ($p>0.05$).

	F	F+L	P	P+L	D	D+L
PS-OCT (dB·μm) (n=10)	1154(679) a,b	716(257) b,c,d	272(162) c	590(235) c,d	1468(499) a	899(431) b,d
TMR (vol%·μm) (n=9)	1903(2256) a,b	41(335) a	—	—	3770(3768) b	276(408) a
PLM (μm) (n=8)	82(44) a	27(12) b,c	—	20(4) b	146(41) d	70(67) a,c
LIF contrast (n=10)	0.54(0.17) a	0.36(0.18) a,b	—	0.10(0.10) b	0.50(0.31) a,c	0.25(0.23) b,c

well as distinguish between regions treated only with the laser (D+L) versus the untreated region. PS-OCT was unable to detect a significant difference between laser plus fluoride (F+L), fluoride (F), and laser only (D+L) groups, nor could PS-OCT significantly distinguish between fluoride (F) and untreated (D) regions. The differences in integrated reflectivity of the protected laser (P+L) and sound enamel (P) regions were also not statistically significant ($p>0.05$). This was surprising because on many of the PS-OCT images, the laser-treated enamel was readily visible. This is likely due to the relatively shallow depth of the modified enamel in comparison to the integration depth of 200 μm.

As anticipated, the severity of the lesions generated in the bovine enamel samples were more severe than for the human enamel samples and we were able to better discriminate significant statistical differences between treatment groups for the bovine samples. Although bovine enamel is structurally similar to human enamel, bovine enamel is more porous and more susceptible to demineralization as well as fluoride absorption; thus, the effects of lesion-inhibiting treatments are more pronounced. For example, there was a significant difference between the (F) and (F+L) regions for the bovine samples, but not for the human samples prior to subtracting the reflectivity from the sound areas.

The integrated mineral loss or ΔZ values and the lesion depth measured with PLM for both the human and bovine enamel groups are plotted in Figs. 9 and 10, respectively. These measurements were taken from the 200-μm-thick transverse sections cut from the samples. For the bovine samples, both TMR and PLM indicated significant differences between laser-treated regions, (F+L) and (D+L), versus untreated areas (D). Interestingly, both TMR and PLM were able to detect a significance difference between the fluoride area (F) and the untreated area (D). However, this apparent higher sensitivity is most likely due to specimen damage in lesion areas during the sectioning process. Because areas of lesion

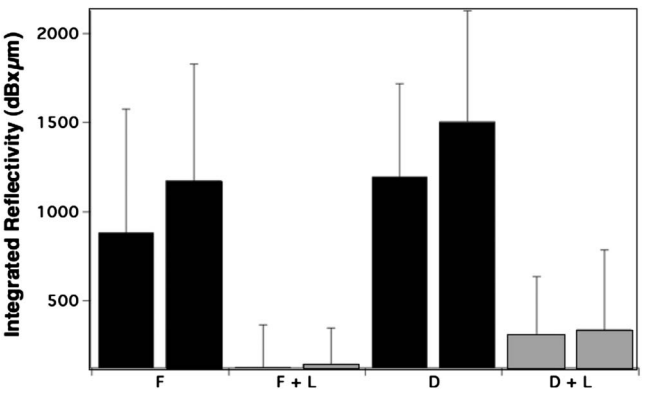

Fig. 8 Mean (s.d) values of the integrated reflectivity or ΔR for bovine and human enamel samples imaged with PS-OCT including four of the treatment groups after subtraction of the (sound+laser) or (sound) reflectivity. The integrated reflectivity was calculated to a depth of 200 μm. The data are paired with the human enamel bars on the left and bovine enamel bars on the right. Bars sharing the same color or pattern among each enamel type, bovine or human, are not significantly different ($p>0.05$).

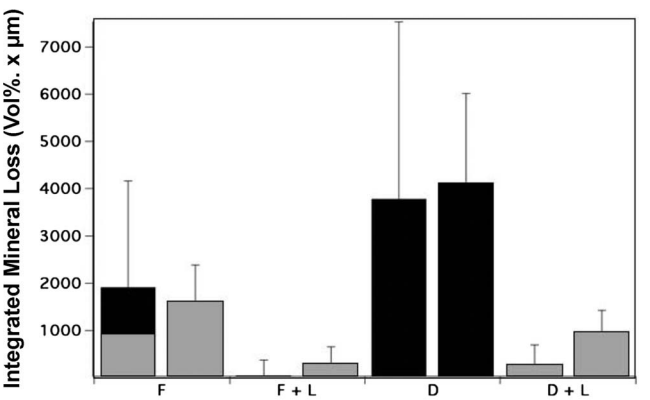

Fig. 9 Mean (s.d) values of the integrated mineral loss or ΔZ for bovine and human enamel samples imaged using TMR including four of the treatment groups. The integrated mineral loss was calculated to a depth of 200 μm. The data are paired with the human enamel bars on the left and bovine enamel bars on the right. Bars sharing the same color or pattern among each enamel type, bovine or human, are not significantly different ($p>0.05$).

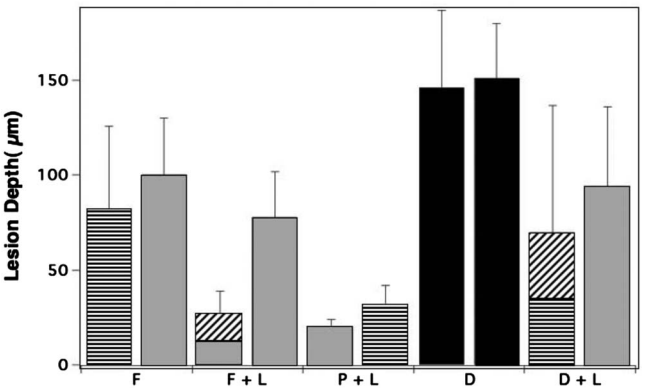

Fig. 10 Mean (s.d) values of the lesion depth in microns for bovine and human enamel samples measured with PLM including five of the treatment groups. The data are paired with the human enamel bars on the left and bovine enamel bars on the right. Bars sharing the same color or pattern among each enamel type, bovine or human, are not significantly different ($p>0.05$).

loss/cavitation are counted as 20% mineral in the calculation of the integrated mineral loss, damage to the very fragile lesion areas that may contain mineral content of >20% (see Fig. 5) leads to an overestimation of the mineral loss by TMR. Therefore, the ΔZ values in more severe lesion areas, such as group (D), are most likely considerably inflated. The fluorescence contrast is plotted in Fig. 11 for both human and bovine enamel. There were significant differences between the laser-treated areas and the nontreated areas for bovine enamel; however, LIF was not very successful in discriminating between the fluoride (F) and lesion only areas (D). For human enamel, LIF was not successful in discriminating a significant difference between the (D) and (D+L) groups.

4 Discussion

The purpose of this study was to determine whether PS-OCT—a nondestructive optical imaging tool—can be used to resolve significant differences in the severity of demineralization on areas treated by a CO_2 laser after exposure to a regimen of artificial demineralization. The laser thermally modifies the enamel to render it more resistant to demineralization; however, those thermal changes also modify the reflectivity and optical appearance of the enamel that may confound accurate assessment of lesion severity. We have also examined the influence of applying fluoride to both laser-treated and untreated areas. The fluoride serves as a positive control and also as a treatment group because several studies have shown a synergistic effect between laser and fluoride treatments. PS-OCT was able to discriminate between the laser-treated and lesion groups on both human enamel and bovine enamel specimens, even without the subtraction of the background reflectivity from sound areas.

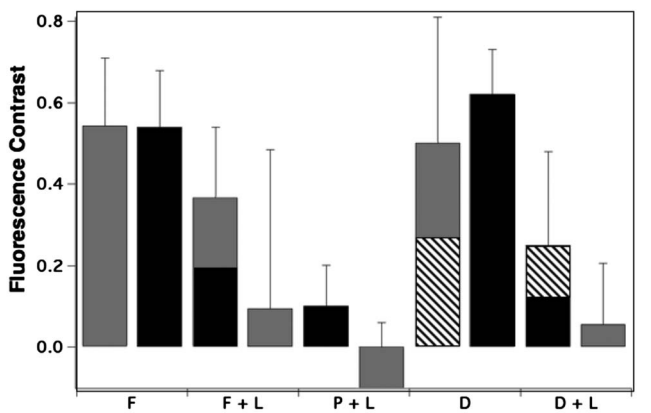

Fig. 11 Mean (s.d) values of the fluorescence contrast for bovine and human enamel samples including five of the treatment groups compared to sound enamel. The data are paired with the human enamel bars on the left and bovine enamel bars on the right. Bars sharing the same color or pattern among each enamel type, bovine or human, are not significantly different ($p>0.05$).

It is interesting that we found there was inhibition of demineralization at the wings of the laser intensity distribution where the enamel surface was not visibly changed by the laser. This suggests that it may be feasible to sufficiently modify the enamel for caries inhibition without changing the appearance of the enamel. The phase transformation of carbonated apatite to the more resistant purer phase hydroxyapatite is a multistage process that is initiated at 420°C, and complete carbonate loss occurs near the melting point of enamel near 1280°C.[7,32,33] Additional studies are needed to determine if it is feasible to control the incident fluence at a level that sufficiently modifies the enamel over large uniform areas without significantly altering the enamel reflectivity.

The most obvious advantage of optical coherence tomography over existing methods of assessing the severity of early demineralization is the potential for *in vivo* imaging because this method is nondestructive. PS-OCT is also advantageous for *in vitro* dissolution studies on extracted teeth because it is difficult to acquire transverse sections through lesion areas without damaging the very fragile lesions for PLM and TMR analysis. Although TMR is considered the gold standard for assessing lesion severity, it is not very sensitive and optical techniques, such as LIF, PS-OCT, and PLM, are better suited for assessing early demineralization. There are also difficulties in accurately assessing the mineral density in the outer 50 μm of enamel due to the tooth curvature. The error caused by the surface curvature can be overcome to some degree by subtracting line profiles in lesion areas from a line profile in the sound area on the same section; however, this still introduces some error. PLM is superior to TMR for measuring lesion depth due to the much higher sensitivity to mineral loss; however, it is very difficult to get a quantitative estimate of the mineral loss from PLM.

Because QLF or LIF has been advocated as a nondestructive tool to assess early demineralization and commercial systems are now available for this purpose, it is valuable to compare this method with PS-OCT. An obvious advantage of QLF is the ability to acquire images of the entire surface of interest even though there is no depth-resolved information. However, simple visible examination or reflected light images of the enamel surface, such as Figs. 2(a) and 4(a), also show contrast between sound and demineralized in a similar manner to QLF albeit with reduced contrast. Therefore, one can always use reflected light images or visible examination to guide the position of the OCT scans. In addition, new high-speed OCT systems are now available that are fast enough to acquire 3-D OCT images at video rates over large areas of the tooth.

In this study, we chose to use both bovine and human enamel specimens for investigation. Bovine enamel is more uniform in composition; however, it is more porous and typically manifests a greater rate of demineralization versus human enamel. Moreover, the greater porosity may influence the performance of topical fluoride because fluoride adheres better to rougher and more porous surfaces. We also observed greater variability among the human samples versus the bovine enamel. This greater variation in the susceptibility of the human enamel samples to demineralization may be caused by previous exposure to fluoride in the oral environment. Even with the smaller lesions and greater variability in susceptibility to dissolution, the benefit of laser irradiation with and without fluoride treatment were still obvious for the human enamel samples. In conclusion, these studies have shown that PS-OCT can be used to assess demineralization in areas irradiated by a CO_2 laser and therefore can be used to assess the efficacy of CO_2 laser treatments *in vivo* without the need to extract the teeth for more conventional assessment using TMR or PLM. Future studies will investigate the use of PS-OCT to assess the inhibition of demineralization at laser irradiation intensities sufficient to remove/ablate enamel and in areas that are subsequently filled with sealants and restorative materials after laser-treatment.

Acknowledgments

Supported by Grants No. NIH/NIDR R01-DE14698, No. R01-DE14554, and No. R01-DE17869. The authors thank Chi Ho, Saman Manesh, and John Featherstone for their help with these studies.

References

1. R. H. Stern, R. F. Sognnaes, and F. Goodman, "Laser effect on *in vitro* enamel permeability and solubility," *J. Am. Dent. Assoc.* **78**, 838–843 (1966).
2. J. D. B. Featherstone and D. G. A. Nelson, "Laser effects on dental hard tissue," *Adv. Dent. Res.* **1**, 21–26 (1987).
3. B. Fowler and S. Kuroda, "Changes in heated and in laser-irradiated human tooth enamel and their probable effects on solubility," *Calcif. Tissue Int.* **38**, 197–208 (1986).
4. S. Kuroda and B. O. Fowler, "Compositional, structural and phase changes in *in vitro* laser-irradiated human tooth enamel," *Calcif. Tissue Int.* **36**, 361–369 (1984).
5. D. G. A. Nelson, M. Shariati, R. Glena, C. P. Shields, and J. D. B. Featherstone, "Effect of pulsed low energy infrared laser irradiation on artificial caries-like lesion formation," *Caries Res.* **20**, 289–299 (1986).
6. J. D. B. Featherstone, N. A. Barrett-Vespone, D. Fried, Z. Kantorowitz, and J. Lofthouse, "CO_2 laser inhibition of artificial caries-like lesion progression in dental enamel," *J. Dent. Res.* **77**, 1397–1403 (1998).
7. J. D. B. Featherstone, D. Fried, and E. R. Bitten, "Mechanism of laser induced solubility reduction of dental enamel," *Proc. SPIE* **2973**, 112–116 (1997).
8. S. Tagomori and T. Morioka, "Combined effects of laser and fluoride on acid resistance of human dental enamel," *Caries Res.* **23**, 225–251 (1989).
9. M. Nobre dos Santos, J. Featherstone, and D. Fried, "Effect of a new carbon dioxide laser and fluoride on sound and demineralized enamel," *Proc. SPIE* **4249**, 87–91 (2001).
10. J. D. B. Featherstone, M. Nobre dos Santos, and D. Fried, "Effect of a new carbon dioxide laser and fluoride on occlusal caries progression in dental enamel," *Proc. SPIE* **4610**, 132–139 (2002).
11. J. L. Fox, D. Yu, M. Otsuka, W. I. Higuchi, J. Wong, and G. L. Powell, "The combined effects of laser irradiation and chemical inhibitors on the dissolution of dental enamel," *Caries Res.* **26**, 333–339 (1992).
12. S. L. Chong, C. L. Darling, and D. Fried, "Nondestructive measurement of the inhibition of demineralization on smooth surfaces using polarization-sensitive optical coherence tomography," *Lasers Surg. Med.* **39**, 422–427 (2007).
13. D. Huang, E. A. Swanson, C. P. Lin, J. S. Schuman, W. G. Stinson, W. Chang, M. R. Hee, T. Flotte, K. Gregory, C. A. Puliafito, and J. G. Fujimoto, "Optical coherence tomography," *Science* **254**, 1178–1181 (1991).
14. B. E. Bouma and G. J. Tearney, Eds., *Handbook of Optical Coherence Tomography*, Marcel Dekker, New York (2002).
15. M. Brezinski, *Optical Coherence Tomography: Principles and Applications*, Elsevier, London (2006).
16. M. R. Hee, D. Huang, E. A. Swanson, and J. G. Fujimoto, "Polarization-sensitive low-coherence reflectometer for birefringence characterization and imaging," *J. Opt. Soc. Am. B* **9**, 903–908 (1992).
17. D. Fried, J. Xie, S. Shafi, J. Featherstone, T. M. Breunig, and C. Q. Le, "Imaging caries lesions and lesion progression with polarization optical coherence tomography," *Proc. SPIE* **4610**, 113–124 (2002).
18. R. S. Jones, M. Staninec, and D. Fried, "Imaging artificial caries under composite sealants and restorations," *J. Biomed. Opt.* **9**, 1297–1304 (2004).
19. R. S. Jones, C. L. Darling, J. D. B. Featherstone, and D. Fried, "Imaging artificial occlusal caries on occlusal surfaces with polarization optical coherence tomography," *Caries Res.* **81–89** (2004).
20. R. S. Jones and D. Fried, "The effect of high index liquids on PS-OCT imaging of dental caries," *Proc. SPIE* **5687**, 34–41 (2005).
21. P. Ngaotheppitak, C. L. Darling, and D. Fried, "Polarization optical coherence tomography for the measuring the severity of caries lesion," *Lasers Surg. Med.* **37**, 78–88 (2005).
22. M. Ando, A. F. Hall, G. J. Eckert, B. R. Schemehorn, M. Analoui, and G. K. Stookey, "Relative ability of laser fluorescence techniques to quantitate early mineral loss *in vitro*," *Caries Res.* **31**, 125–131 (1997).
23. U. Hafstroem-Bjoerkman, E. de Josselin de Jong, A. Oliveby, and B. Angmar-Mansson, "Comparison of laser fluorescence and longitudinal microradiography for quantitative assessment of *in vitro* enamel caries.," *Caries Res.* **26**, 241–247 (1992).
24. B. A. Angmar-Masson, S. Al-Khateeb, and S. Tranaeus, "Intraoral use of quantitative light-induced fluorescence detection method," *Early Detection of Dental Caries*, pp. 39–50, Indiana University, Indianapolis (1996).
25. M. D. Lagerweij, M. H. van der Veen, M. Ando, and L. Lukantsova, "The validity and repeatability of three light-induced fluorescence systems: An *in vitro* study," *Caries Res.* **33**, 220–226 (1999).
26. H. Eggertsson, M. Analoui, M. H. v. d. Veen, C. Gonzalez-Cabezas, G. J. Eckert, and G. K. Stookey, "Detection of early interproximal caries *in vitro* using laser fluorescence, dye-enhanced laser fluorescence and direct visual examination," *Caries Res.* **33**, 227–233 (1999).
27. E. de Josselin de Jong, F. Sundstrom, H. Westerling, S. Tranaeus, J. J. ten Bosch, and B. Angmar-Mansson, "A new method for *in vivo* quantification of changes in initial enamel caries with laser fluorescence," *Caries Res.* **29**, 2–7 (1995).
28. M. H. van der Veen, E. de Josselin de Jong, and S. Al-Kateeb, "Caries activity detection by dehydration with qualitative light fluorescence," *Early detection of Dental caries II*, Vol. **4**, pp. 251–260, Indiana University, Indianapolis (1999).
29. G. K. Stookey, *Quantitative Light Fluorescence: A Technology for Early Monitoring of the Caries Process*, Vol. **49** W. B. Saunders, Philadelphia (2005).
30. J. J. ten Bosch, "Summary of research of quantitative light fluorescence," *Early Detection of Dental Caries II*, Vol. **4**, pp. 261–278, Indiana University, Indianapolis (1999).
31. D. Fried, J. Xie, S. Shafi, J. D. B. Featherstone, T. Breunig, and C. Q. Lee, "Early detection of dental caries and lesion progression with polarization sensitive optical coherence tomography," *J. Biomed. Opt.* **7**, 618–627 (2002).
32. D. W. Holcomb and R. A. Young, "Thermal decomposition of human tooth enamel," *Calcif. Tissue Int.* **31**, 189–201 (1980).
33. M. Zuerlein, D. Fried, and J. D. B. Featherstone, "Modeling the modification depth of carbon dioxide laser treated enamel," *Lasers Surg. Med.* **25**, 335–347 (1999).